BRAIN COMMUNICATIONS

Novel translational phenotypes and biomarkers for creatine transporter deficiency

Raffaele Mazziotti,[1,2]* Francesco Cacciante,[3]* Giulia Sagona,[1,4]* Leonardo Lupori,[3] Mariangela Gennaro,[2] Elena Putignano,[2] Maria Grazia Alessandrì,[4] Annarita Ferrari,[4] Roberta Battini,[4,5] Giovanni Cioni,[4,5] Tommaso Pizzorusso[1,2] and Laura Baroncelli[2,4]

*These authors contributed equally to this work.

Creatine transporter deficiency is a metabolic disorder characterized by intellectual disability, autistic-like behaviour and epilepsy. There is currently no cure for creatine transporter deficiency, and reliable biomarkers of translational value for monitoring disease progression and response to therapeutics are sorely lacking. Here, we found that mice lacking functional creatine transporter display a significant alteration of neural oscillations in the EEG and a severe epileptic phenotype that are recapitulated in patients with creatine transporter deficiency. In-depth examination of knockout mice for creatine transporter also revealed that a decrease in EEG theta power is predictive of the manifestation of spontaneous seizures, a frequency that is similarly affected in patients compared to healthy controls. In addition, knockout mice have a highly specific increase in haemodynamic responses in the cerebral cortex following sensory stimuli. Principal component and Random Forest analyses highlighted that these functional variables exhibit a high performance in discriminating between pathological and healthy phenotype. Overall, our findings identify novel, translational and non-invasive biomarkers for the analysis of brain function in creatine transporter deficiency, providing a very reliable protocol to longitudinally monitor the efficacy of potential therapeutic strategies in preclinical, and possibly clinical, studies.

1 Department of Neuroscience, Psychology, Drug Research and Child Health NEUROFARBA, University of Florence, Florence I-50135, Italy
2 Institute of Neuroscience, National Research Council (CNR), Pisa I-56124, Italy
3 BIO@SNS Lab, Scuola Normale Superiore di Pisa, Pisa I-56125, Italy
4 Department of Developmental Neuroscience, IRCCS Stella Maris Foundation, Pisa I-56128, Italy
5 Department of Clinical and Experimental Medicine, University of Pisa, Pisa I-56126, Italy

Correspondence to: Laura Baroncelli, PhD Institute of Neuroscience, National Research Council (CNR), via Moruzzi 1, Pisa I-56124, Italy, E-mail: baroncelli@in.cnr.it

Keywords: creatine transporter deficiency; biomarkers; epilepsy; EEG; optical imaging

Abbreviations: Cr = creatine; CrT = Cr transporter 1; IOS = intrinsic optical signal; PND = postnatal day; WT = wild-type

Received March 21, 2020. Revised May 20, 2020. Accepted June 10, 2020. Advance Access publication July 3, 2020

Graphical Abstract

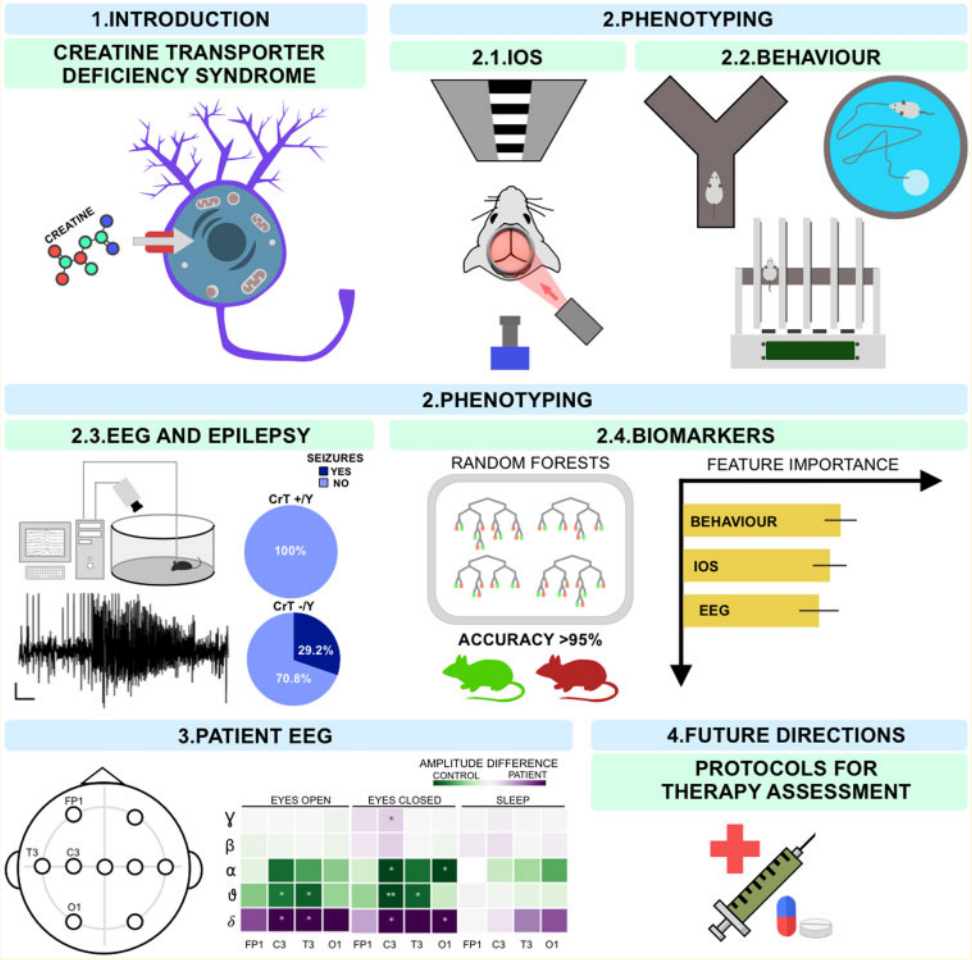

Introduction

A disruption of brain energy metabolism has been associated with multiple psychiatric and neurological disorders, including for instance schizophrenia, Rett syndrome and a subset of autism spectrum disorders (e.g. Müller and Can, 2014; Rose *et al.*, 2018; Dwir *et al.*, 2019). Creatine (Cr) transporter deficiency is a recessive X-linked inherited alteration of metabolism (OMIM #300352), characterized by greatly diminished or undetectable levels of Cr in the brain, and presenting with early intellectual disability, symptoms overlapping with autism spectrum disorders, seizures and motor abnormalities (Cecil *et al.*, 2001; van de Kamp *et al.*, 2014). Creatine transporter deficiency is caused by mutations in *Slc6a8* gene and loss of function of Cr transporter 1 (CrT), which transports Cr both across the blood–brain barrier and into the cells (Nash *et al.*, 1994). The prevalence of creatine transporter deficiency is unknown, but the disorder has been estimated to account for 1–2% of males with non-syndromic mental disability (van de Kamp *et al.*, 2014). Although rare, creatine transporter deficiency represents a major issue in health care, as it is a chronic illness requiring lifelong care and resulting in a large impact on the quality of life of both patients and caregivers, as well as a burden on the healthcare system. There are no therapies for this disorder and the current standard of care is a palliative approach for managing seizures and behavioural problems (van de Kamp *et al.*, 2014). Previous attempts to rescue Cr content in the brain of creatine transporter deficiency patients by exploiting nutritional supplements or Cr analogues have met with very limited success (Chilosi *et al.*, 2008; Mercimek-Mahmutoglu *et al.*, 2010; Kurosawa *et al.*, 2012; Valayannopoulos *et al.*, 2012; Dunbar *et al.*, 2014; Jaggumantri *et al.*, 2015). Recently, CrT knockout murine models that recapitulate many aspects of the human disease have become available, supporting the preclinical development of therapeutics and a better understanding of creatine transporter deficiency pathophysiology (Skelton *et al.*, 2011; Kurosawa *et al.*, 2012; Baroncelli *et al.*, 2016: Udobi *et al.*, 2018; Molinaro *et al.*, 2019). However, the efficacy study of novel potential treatments is hindered by

the scarcity of unbiased, quantitative biomarkers for monitoring brain development and function.

EEG and sensory-evoked responses are readily applicable to humans and widely used for non-invasive assessment of cortical function, making electrophysiological measurements or functional imaging ecologically ideal translational tools for functional analyses in children with neurodevelopmental disorders (Nelson and McCleery, 2008; Lloyd-Fox *et al.*, 2010; Vanderwert and Nelson, 2014). Accordingly, previous studies reported that a standardized inspection of EEG and cortical responses to sensory stimuli is suitable to reveal, in both animal models and patients, stage-specific alterations in other disorders affecting neurodevelopment (Bosl *et al.*, 2011; Durand *et al.*, 2012; LeBlanc *et al.*, 2015; Boggio *et al.*, 2016; Mazziotti *et al.*, 2017; Bowman and Varcin, 2018; Lupori *et al.*, 2019). Abnormal EEG waveforms have been previously documented in creatine transporter deficiency patients, indicating diffuse slowing, interictal theta activity, specific sharp abnormalities and focal/generalized paroxysmal or slow abnormalities (Schiaffino *et al.*, 2005; Póo-Argüelles *et al.*, 2006; Mancardi *et al.*, 2007; Fons *et al.*, 2009; Leuzzi *et al.*, 2013). However, a quantitative examination of creatine transporter deficiency electroclinical features is still missing.

Here, we performed an extensive functional analysis in knockout mice lacking CrT ($CrT^{-/y}$) and creatine transporter deficiency patients identifying reliable biomarkers that could potentially be used to evaluate therapeutics pre-clinically as well as clinically.

Materials and methods

Animals

We used male mice hemizygous for CrT exons 5–7 deletion ($CrT^{-/y}$ or knockout) on a C57Bl6J background (Baroncelli *et al.*, 2014), and their wild-type (WT; $CrT^{+/y}$) littermates. Animals in each experimental group came from different litters, with a minimum of three litters to prevent possible litter effects. Animals were maintained at 22°C under a 12-h light–dark cycle (average illumination levels of 1.2 cd/m^2) and housed in standard cages according to current regulations about animal welfare. Food (4RF25 GLP Certificate, Mucedola) and water were available *ad libitum*. Genomic DNA was isolated from mouse tail (Dneasy Blood and Tissue Kit, Qiagen, USA) and genotyping was performed as previously described (Baroncelli *et al.*, 2014). All experiments were carried out in accordance with the European Directive of 22 September 2010 (EU/63/2010) and were approved by the Italian Ministry of Health (authorization number 507/2018-PR).

EEG recordings in mice

A two-channel headmount (8201, Pinnacle Technology) for EEG recordings was placed on the skull of mice anaesthetized with isoflurane (1–3%). EEG electrodes were stainless steel screws implanted epidurally over the frontal and the occipital areas. EEG signals were recorded using a preamplifier (8202-SL) connected to a data acquisition system (8206, Pinnacle Technology) and Sirenia Software 1.7.9 (Pinnacle Technology). Signals were recorded at 400 Hz sampling frequency to evaluate baseline (spontaneous) activity for 24 h followed by treatment with intraperitoneal kainic acid at 10 mg/kg to evoke seizure activity. Video was recorded in parallel during the entire duration of the EEG assessments. For the analysis of baseline EEG, signals were segmented in 30 s epochs. The vigilance state in each epoch was manually classified as active wake, passive wake or sleep, based on the inspection of video recordings by an operator blind to the genotypes. EEG signals were converted into power spectra by Fast Fourier Transform for at least 12 epochs in each light/dark cycle and wake/sleep condition. Consecutive epochs of the same vigilance state were selected to be spaced at least 10 min apart between each other. The spectra were normalized to the total power of the signal. The power spectra were averaged over subjects in each light/dark cycle and wake/sleep condition at frequency ranges divided into five bands as follows: 0.5–4 (delta), 4–8 (theta), 8–12 (alpha), 12–30 (beta) and 30–45 (gamma) Hz (Kadam *et al.*, 2017). A correlation matrix of EEG spectral power in $CrT^{-/y}$ and WT animals was obtained using Spearman correlation, with Benjamini–Hochberg adjustment (Python, *scipy* library). To quantify both baseline (spontaneous) and kainic acid-evoked seizure episodes we used Sirenia Seizure Pro 1.8.4 (Pinnacle Technology). The baseline period of each animal was used as a cut-off threshold (mean line length + 8 × standard deviation). Events in the 2–10 Hz frequency range, with a line length higher than the defined threshold, and lasting at least 10 s were identified as seizures. At the behavioural level, seizures were scored according to Racine scale (Racine, 1972). Seizures of stage 1 and 2 were classified as tonic events, seizures of stage 3 were assigned to clonic events and seizures of stage 4, 5 and 6 were categorized as tonic–clonic events.

Patients

Five subjects with creatine transporter deficiency aged to the present date between 7.7 and 22.7 years were diagnosed at IRCCS Stella Maris Foundation at the age ranging between 5.1 and 9 years (mean age = 7.2 years; standard deviation = 1.8 years). All patients showing clinical, neurochemical (Cr/creatinine urine levels and lack of brain Cr at ^{1H}magnetic resonance spectroscopy) and genetical diagnosis of creatine transporter deficiency have been recruited in this study and matched with 12 healthy

Table 1 Clinical and demographic characteristics of patients with creatine transporter deficiency

Patient no./gender	Age (years)/seizure type at onset	Age (years) at EEG	Age (years) at last follow-up	Biochemical value (Cr/Crn; n.v. < 1.0)	Genetic testing (*Slc6a8* mutation)
1/M	5.0/ focal motor	8.4	22.7	2.35	c. 1006-1008 del AAC (*de novo*)
2/M	0.4/spasms	8.3	15.8	3.6	IV s1-2A >G
3/M	No seizures	5.5	15.6	3.08	c.757 G>C (inherited)
4/M	No seizures	9.0	8.3	2.12	p.Val246Cysfs*47
5/M	1.3/focal to bilateral	5.1	7.5	3.5	c.1376T>C, p. Leu459Pro

Crn: creatinine; M: male.

subjects. The mean age of controls was 7.7 years (standard deviation = 2.3 years). A breakdown of demographics for creatine transporter deficiency patients is reported in Table 1. Data have been anonymized using an alphanumeric code. Despite the occurrence of seizures with predominant focal onset in patients 1, 2 and 5, no specific EEG pattern can be recognized in the clinical observation of interictal video-EEG. The experiment has been subjected to approval by the Ethics Board (201/2019, Pediatric Ethics Board of Tuscany) and has been performed in accordance with the Declaration of Helsinki.

EEG recordings in patients

EEG recordings were performed as part of routine examination of patients with intellectual disability and language deficits. Data were collected using a Micromed or Grass EEG recording system. Gold ring electrodes were placed following the international 10–20 convention for a 32-channel cap and signals were recorded at a sampling rate of 500 Hz. For this analysis, we used the first EEG recorded at the time of diagnosis; thus, patients were not prescribed yet anticonvulsant medications. The spectral power values in the same frequency bands described above for mice were evaluated in humans (Kadam *et al.*, 2017). EEG recordings were screened and divided into artefact-free segments (10 s duration for eyes closed condition, 20 s duration for eyes open and sleep conditions). EEG signal was then exported in European Data Format and subjected to Fast Fourier Transform. Power spectra were estimated by averaging at least 8 segments for each behavioural state. The spectra were normalized to the total power of the signal. Data analysis was performed by an operator blind to the genotype.

Intrinsic optical signal imaging and visually evoked potentials

Surgery was performed as previously described (Mazziotti *et al.*, 2017). Isoflurane was used as anaesthesia. A thin layer of cyanoacrylate was poured over the exposed skull to affix a custom-made metal ring (9 mm internal diameter) in correspondence to the binocular visual cortex and a drop of transparent nail polish was used to improve the optical access. Intrinsic optical signal (IOS) imaging recordings were performed under isoflurane (0.5–1%) and chlorprothixene anaesthesia (1.5 mg/kg, intraperitoneal) longitudinally in each animal at postnatal day (PND) 40, PND110 and PND180. Images were visualized using a custom Leica microscope (Leica Microsystems). The animals were secured under the objective using a ring-shaped magnet mounted on an Arduino-based imaging chamber. Red light illumination (630 nm) was obtained with 8 individually addressable light emitting diodes (WS2812) fixed to the objective (Leica Z6 APO coupled with a Leica PanApo 2.0X 10447170) by a custom 3D printed conical holder (Lupori *et al.*, 2019). Visual stimuli were generated using Matlab Psychtoolbox and presented on a monitor placed 13 cm away from the eyes of the mouse. Sinusoidal wave gratings were presented in the binocular portion of the visual field with spatial frequency 0.03 cyc/deg, mean luminance 20 cd/m^2 and contrast up to 90%. The stimulus consisted in the abrupt contrast reversal of a grating with a temporal frequency of 4 Hz for 1 s. Frames were acquired at 30 fps with a resolution of 512 × 512 pixels. The signal was averaged for at least 80 trials. Fluctuations of reflectance (R) for each pixel were computed as the normalized difference from the average baseline (ΔR/R). A region of interest was calculated on the mean image of contralateral eye response by selecting the pixels in the lowest 30% ΔR/R of the range between the maximal and minimal intensity pixels, and mean evoked response was quantitatively estimated as the average intensity within the region of interest. [See Mazziotti *et al.* (2017) for further details on signal analysis.] A separate group of animals were used for visually evoked potential experiments at PND110 using Cheetah 32 (Neuralynx) recording system (Mazziotti *et al.*, 2017).

Behavioural tests

All behavioural tests were performed as previously reported (Baroncelli *et al.*, 2016).

Y maze: we used a Y-shaped maze with three symmetrical plastic arms at a 120-degree angle (26 cm × 10 cm × 15 cm). Mice were allowed to freely explore the maze for 8 min. Video recordings (Noldus Ethovision XT) were used for offline blind analysis. An arm entry was defined as all four limbs within the arm. A triad was defined as a set of three arm entries, when each entry was to a different arm of the maze. The

number of arm entries and the number of triads were recorded to calculate the alternation percentage. *Morris water maze*: mice were trained for four trials per day and for a total of 7 days in a circular water tank (diameter, 120 cm; height, 40 cm), filled to a depth of 25 cm with water (21–22°C) added with atoxic white paint. Four alternative starting positions defined the division of the tank into four quadrants. A square clear Perspex platform (11 cm × 11 cm) was submerged 0.5 cm below the water surface and placed at the midpoint of the target quadrant. Mice were allowed up to 60 s to locate the escape platform, and their swimming paths were recorded by the Noldus Ethovision system. On the last trial (probe trial), the platform was removed and the swimming paths were recorded over 60 s. *Rotarod*: mice were placed on a drum with increasing rotation speed from 4 to 40 rpm in 10 min. The time spent on the drum was recorded by an automated unit. Four consecutive trials with an inter-trial interval of 5 min were performed in the same day.

Experimental design

The same animals were subjected to longitudinal IOS recordings at PND40, PND110 and PND180. At least 4 days after the completion of each IOS recording, the animals were each subjected to serial neurobehavioural assessments of cognitive and psychomotor functions [Y maze, Rotarod, Morris Water Maze (PND110 and PND180 only)]. At the end of the experimental schedule (PND200), EEG recordings were performed. Data analysis was performed *a posteriori* by an operator blind to the genotype of mice.

Machine learning-based classification

Scikit-learn, a Python-based library (http://scikit-learn.org/stable/), was used to compute both principal component analysis and train the classification model. The model is a supervised machine learning algorithm called Random Forest that is based on multiple decision tree learning. We used the Scikit-learn implementation for this algorithm, called *ExtraTreesClassifier* function. To determine an optimal set of hyperparameters for the classifier we used the function *RandomizedSearchCV* on the dataset with all the variables. Then, we applied the Random Forest classifier adopting the function *cross_val_score* with cv = 3 to perform 3-fold cross-validation. To calculate feature importance in classifier decision, we used the attribute *feature_importance* that is an instance of the *ExtraTreesClassifier* expressing the fraction of relative importance for each feature. Data from all ages of phenotyping (PND40, PND110 and PND180) were averaged together.

Statistical analysis

For the assessments in mice, we estimated the sample size needed for each experiment by performing a power analysis using G*Power ($\alpha = 0.05$, $\beta = 0.2$). The estimate of the expected difference between the experimental groups was based on the knowledge of values of the studied parameter obtained historically in the same laboratory in $CrT^{-/y}$ animals. For each parameter, we estimated the minimal difference that would be biologically relevant considering the impact of the possible difference on the animals' brain function and behaviour. Considering the rarity of creatine transporter deficiency and the few patients studied herein, we did not perform a specific statistical analysis for the patient assessments. All statistical analyses of the results were performed using GraphPad Prism 8.0.1 and Python. Differences between two groups were assessed with a two-tailed *t*-test. Multiple *t*-test with Benjamini, Krieger and Yekutieli adjustment were used for the analysis of EEG spectral power in mice. Multiple *t*-test were used for the analysis of EEG spectral power in patients. Correlation analysis was obtained using Spearman correlation, with Benjamini–Hochberg adjustment. The significance of factorial effects and differences among more than two groups were evaluated with ANOVA/repeated measures ANOVA followed by *post hoc* Holm–Sidak test. Fisher's exact test and χ^2 test were used to compare sampling distributions. Rank transformation was exploited for data not normally distributed. The level of significance was $P < 0.05$.

Data availability

The datasets generated during this study are available from the corresponding author on reasonable request.

Results

Creatine transporter deficiency causes an alteration of cortical oscillations in mice and humans

We performed 24 h video-EEG recordings in awake, freely moving adult mice with a view to thoroughly examining basal brain activity of WT and $CrT^{-/y}$ animals (Fig. 1a). We found that $CrT^{-/y}$ animals show significantly altered power in a wide range of EEG frequencies, including theta (4–8 Hz), alpha (8–12 Hz), beta (12–30 Hz) and gamma (30–45 Hz) bands, both during active/passive wake and sleep, regardless of the light or dark phase (Fig. 1b and Supplementary Figs 1 and 2). Interestingly, a correlation matrix to summarize spectral density data in WT and $CrT^{-/y}$ mice suggests an anomalous synchronization of brain activity and, possibly, functional connectivity in the brain of $CrT^{-/y}$ animals. Spectral densities in $CrT^{-/y}$ mice showed a lower proportion of positive correlations (blue patches; 59.8% versus 75.8%) and a higher percentage of inversely correlated frequency bands (red patches; 59.8% versus 40.2%) compared to WT animals (Supplementary Fig. 3).

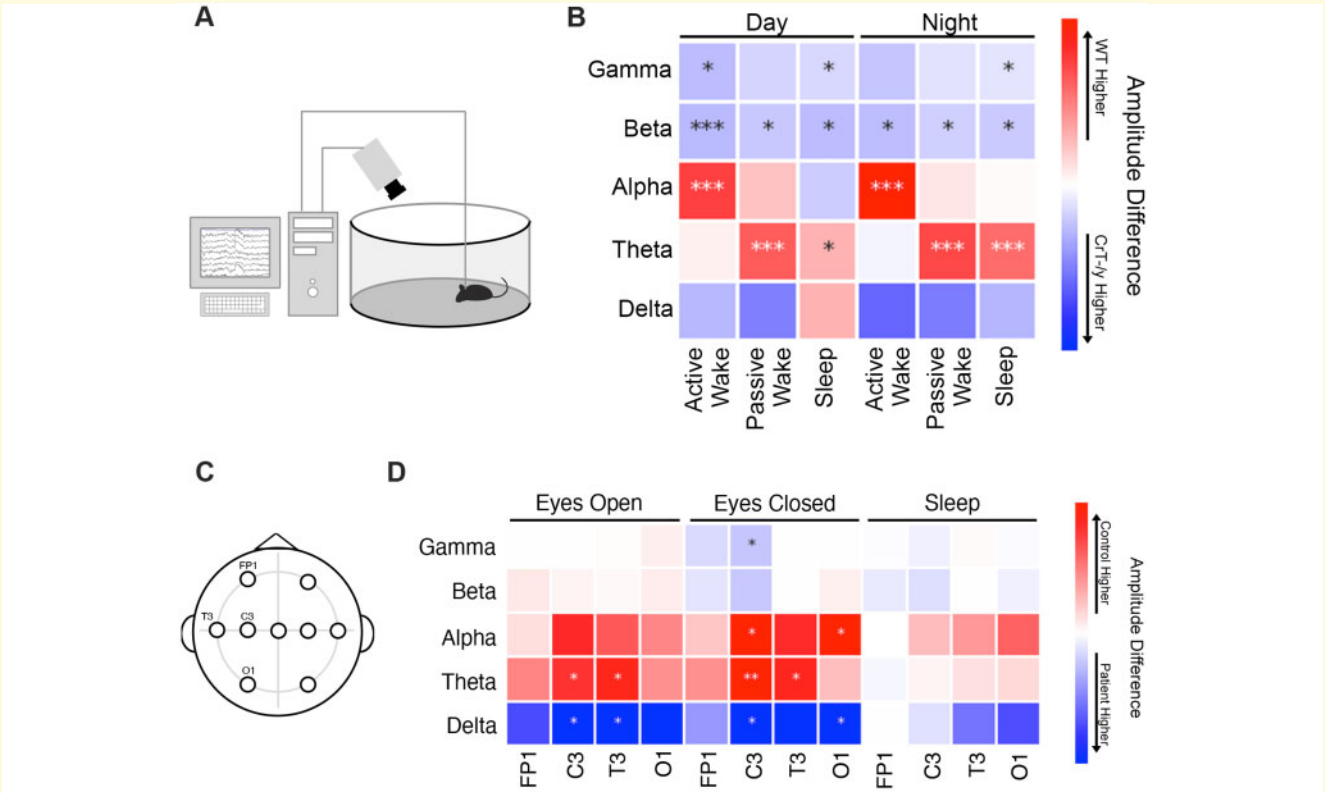

Figure 1 Altered neural oscillations in CrT$^{-/y}$ mice and creatine transporter deficiency patients. (**A**) Schematic diagram of the apparatus used for video-EEG recordings in awake, freely moving mice. EEG recordings were performed at PND200. For baseline EEG analysis, signals were segmented in 30 s epochs. The vigilance state in each epoch was manually classified as active wake, passive wake or sleep, based on the inspection of video recordings. EEG signals were converted into power spectra by Fast Fourier Transform for at least 12 epochs in each light/dark cycle and wake/sleep condition. Consecutive epochs of the same vigilance state were selected to be spaced at least 10 min apart between each other. The spectra were normalized to the total power of the signal. The power spectra were averaged over subjects in each light/dark cycle and wake/sleep condition at frequency ranges divided into five bands as follows: 0.5–4 (delta), 4–8 (theta), 8–12 (alpha), 12–30 (beta) and 30–45 (gamma) Hz. (**B**) The patch colour indicates the relative difference between WT ($n = 22$) and CrT$^{-/y}$ mice ($n = 24$) in the amplitude of EEG power bands, measured in three different behavioural states (active wake, passive wake and sleep) both during the day and the night phase. A single asterisk or a triple asterisk in the coloured patch indicates $P < 0.05$ and $P < 0.001$ (multiple *t*-test, corrected using the Benjamini, Krieger and Yekutieli procedure), respectively. (**C**) Schematic diagram of electrode location in the 10–20 international system for EEG recordings. We used this electrode configuration for EEG recordings in creatine transporter deficiency patients and age-matched controls. The mean age of creatine transporter deficiency patients was 7.2 years (standard deviation = 1.8 years); for controls the mean age was 7.7 years (standard deviation = 2.3 years). Electrodes used for the analysis were FP1 (frontopolar 1), C3 (central 3), T3 (temporal 3) and O1 (occipital 1). EEG recordings were screened and divided into artefact-free segments (10 s duration for eyes closed condition, 20 s duration for eyes open and sleep conditions). EEG signal was then exported in European Data Format and subjected to Fast Fourier Transform. Power spectra were estimated by averaging at least 8 segments for each behavioural state. The spectral power values in the same frequency bands described above for mice were evaluated in humans. The spectra were normalized to the total power of the signal. (**D**) The patch colour indicates the relative difference between healthy controls ($n = 12$) and creatine transporter deficiency patients ($n = 5$) in the amplitude of EEG power bands, measured in three different behavioural states (eyes open, eyes closed and sleep). A single asterisk or a double asterisk in the coloured patch indicates $P < 0.05$ and $P < 0.01$ (multiple *t*-test), respectively. Representative EEG traces and power spectrum plots are also shown.

To obtain a clinical validation of results obtained in the mouse model, we evaluated EEG data from creatine transporter deficiency children diagnosed at the IRCCS Stella Maris Foundation (Fig. 1c). We report a significant difference between creatine transporter deficiency patients and age-matched controls for frequency oscillations in the delta, theta, alpha and gamma bands. These alterations are particularly prominent in the signal recorded from the central 3 electrode, but some of them are recurring at the temporal 3 and occipital 1 recording sites as well (Fig. 1d and Supplementary Figs 4–6).

CrT$^{-/y}$ mice display a spontaneous epileptic phenotype

We found that ~30% of CrT$^{-/y}$ animals showed at least one spontaneous seizure detectable both at behavioural level and as epileptiform activity in EEG during baseline

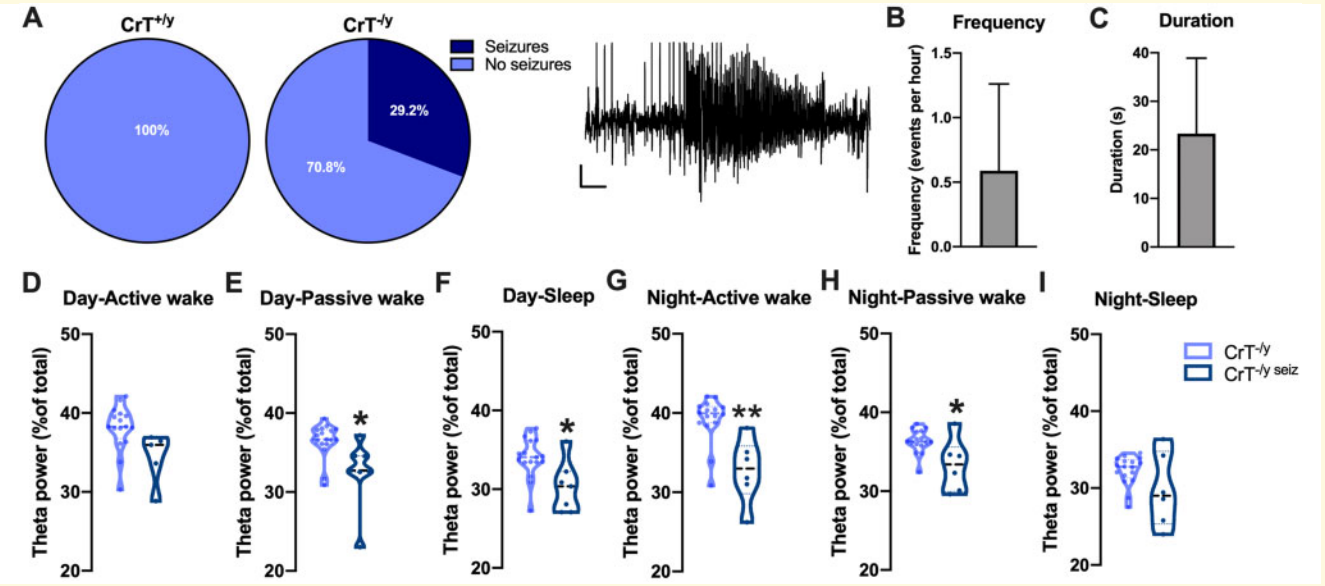

Figure 2 Spontaneous epileptic phenotype in CrT$^{-/y}$ animals and stratification of EEG power data according to this phenotype. (**A**) Using baseline EEG recordings (24 h), we found that 30% of CrT$^{-/y}$ mice ($n = 24$) display spontaneous seizures, while no ictal events were detected in WT animals ($n = 22$). On the right, a representative seizure in a CrT$^{-/y}$ mouse is shown. Calibration bar: 100 μV, 10 s. (**B**) Frequency of spontaneous seizures in CrT$^{-/y}$ epileptic animals. (**C**) Average duration of spontaneous seizures in CrT$^{-/y}$ epileptic animals. (**D–I**) Violin plots with individual values (filled circles) depict normalized theta power spectrum of cortical EEG recordings from epileptic (CrT$^{-/y\ seiz}$, $n = 7$) and non-epileptic CrT$^{-/y}$ mice (CrT$^{-/y}$, $n = 17$). Decreased power of 4–8 Hz theta frequency band in epileptic CrT$^{-/y}$ mice during the passive wakefulness and sleep in the light phase, and during the active and passive wakefulness in the dark phase. Multiple *t*-tests with adjusted *P*-value: $^{*}P < 0.05$, $^{**}P < 0.01$. Error bars, standard deviation.

recording (24 h), whereas no ictal events were detected in WT littermates (Fig. 2a). Notably, CrT$^{-/y}$ mice with the spontaneous epileptic phenotype display on average one electrographical seizure every 2 h (Fig. 2b), with a mean duration of ~20 s (Fig. 2c), that simultaneously presented as clonic or tonic–clonic convulsions at the behavioural level in most cases (1.4% of tonic seizures, 54.3% of clonic seizures, 44.3% of tonic–clonic seizures; Supplementary Videos 1 and 2). The larger portion of spontaneous seizures occurred during passive wake (7.1% during active wake, 62.9% during passive wake, 30.0% during sleep). The stratification of power spectra revealed a specific decrease in theta band in CrT$^{-/y}$ animals displaying spontaneous epilepsy (Fig. 2d–i). Moreover, CrT$^{-/y}$ mice presented a distinct response to kainic acid challenge compared to WT mice. Statistical analysis revealed a significant effect of genotype with a higher Racine behavioural score following kainic acid administration (Fig. 3a), lower latency to epileptiform activity bursts (Fig. 3b) and higher frequency and mean duration of epileptiform bursts in CrT$^{-/y}$ with respect to WT mice (Fig. 3c and d). In addition, the distribution of seizure severity was significantly different between the two groups with CrT$^{-/y}$ mice presenting a high percentage of tonic–clonic seizures (Fig. 3e).

Taken together, these data reveal that CrT$^{-/y}$ mice exhibit spontaneous seizures and increased susceptibility to pro-convulsant treatment. Moreover, the power of theta EEG band in CrT$^{-/y}$ animals appears to be predictive of spontaneous seizures phenotype.

Altered neurovascular coupling is present in CrT$^{-/y}$ mutants

We examined cortical responses to visual stimulation using intact skull IOS imaging in juvenile (PND40) CrT$^{-/y}$ animals. Figure 4a shows typical examples of responses from CrT$^{-/y}$ and age-matched WT littermates. Data analysis revealed that IOS amplitude of the responses driven by contralateral eye stimulation was significantly higher in CrT$^{-/y}$ compared to control mice and the effect was particularly evident at higher contrasts of visual stimuli (Fig. 4b). We longitudinally tracked visual responses in the same animals as they aged using the 90% contrast visual stimuli. The response to the contralateral eye showed a similar pattern at PND110 and PND180 with a significantly increased amplitude in CrT$^{-/y}$ compared to WT mice (Fig. 4c). Moreover, the latency to response peak was higher in CrT$^{-/y}$ at PND110 and PND180 (Fig. 4d). These results show that haemodynamic response is markedly altered in the cortex of mutant animals, and that this phenotype progresses with age. To clarify whether this is related to a corresponding change of ongoing neuronal activity, we assessed visual

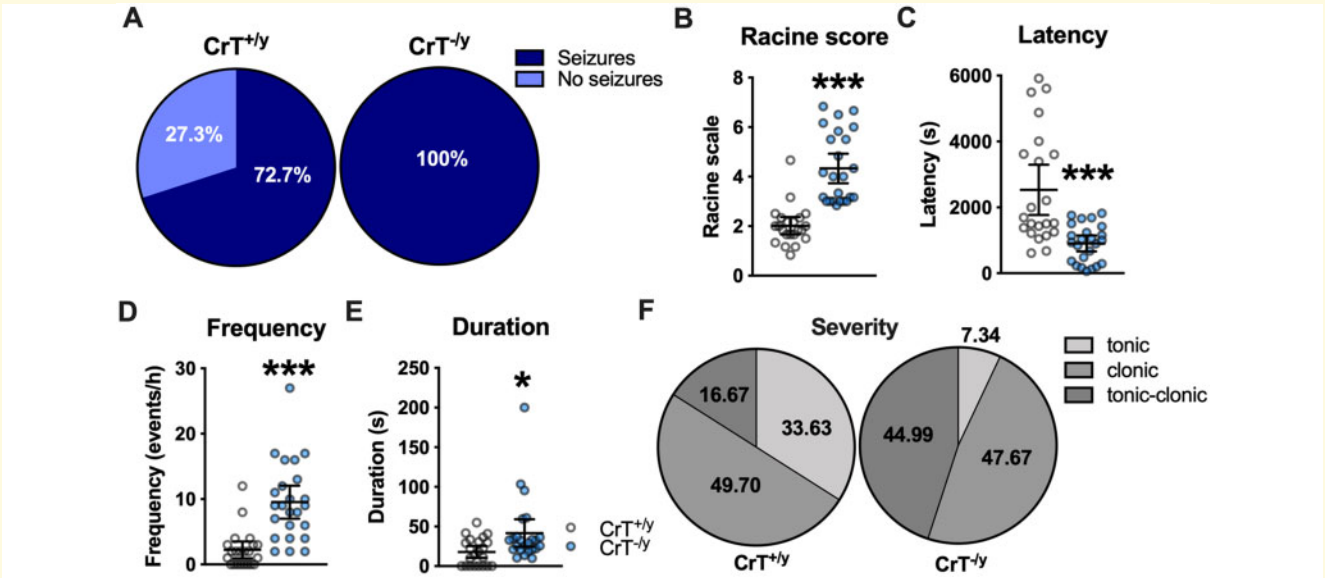

Figure 3 Kainic acid challenge in the brain of CrT$^{-/y}$ mice. (**A**) Kainic acid injection (10 mg/kg) induced overt seizures in 100% of CrT$^{-/y}$ mice ($n = 24$), whereas only 14/22 WT animals displayed epileptic bursts at electrographical level over 1 h of observation. (**B**) Effect of kainic acid treatment at the behavioural level. Circles represent the maximum seizure rating score of individual WT and CrT$^{-/y}$ mice over a period of 1 h after kainic acid administration. Black lines represent mean with 95% confidence interval. CrT$^{-/y}$ mice displayed a higher Racine score (*t*-test, $P < 0.001$). (**C–F**) Severity of kainic acid-induced seizures in WT and CrT$^{-/y}$ mice at electrophysiological level. EEG analysis was performed on the same animals used for behavioural scoring. CrT$^{-/y}$ mice showed a lower latency to the first seizure (**C**, *t*-test, $P < 0.001$), and increased frequency (**D**, *t*-test, $P < 0.001$) and duration (**E**, *t*-test, $P < 0.05$) of seizure events with respect to age-matched littermates. For WT animals not presenting seizures during the 1 h of monitoring, we extended the observation until the occurrence of the first electrographical burst to provide a latency value. Circles represent single data values; black lines indicate mean with 95% confidence interval. Relative percentage of tonic, clonic and tonic–clonic seizures WT and CrT$^{-/y}$ mice (**F**) indicates that seizure severity is more pronounced in CrT$^{-/y}$ animals (χ^2 test; $P < 0.001$). *$P < 0.05$, ***$P < 0.001$.

responses in a separate group of adult (PND110) CrT$^{-/y}$ mice using intracortical visually evoked potential recordings. Data quantification revealed comparable visually evoked potential amplitude and latency in CrT$^{-/y}$ and WT animals (Fig. 4e and f).

A Random Forest classifier quantify robustness of creatine transporter deficiency biomarkers

Longitudinal IOS imaging was conducted along with serial neurobehavioural assessments of cognitive and psychomotor functions (Y maze, Rotarod, Morris Water Maze). At the end of the experimental schedule, EEG recordings were performed in the same animals at PND180. Results of behavioural testing confirmed what was previously reported by our group (Baroncelli *et al.*, 2016; Supplementary Figs 7–9). To evaluate the reliability of the behavioural phenotype, imaging and electrophysiological recordings as biomarkers of creatine transporter deficiency disorder, we computed accuracy using a Random Forest binary classifier, a supervised machine learning algorithm for data classification. When trained with the entire dataset, the algorithm showed a remarkable capability to discriminate between CrT$^{-/y}$ and WT animals (Full; accuracy = 95.67%; Fig. 5b). As a control, we also repeated the procedure after bootstrapping the dataset (Bootstrap; accuracy = 54.86%). We then assessed the discriminative performance of smaller subsets of data dividing the entire dataset in behavioural (Behaviour), imaging (IOS) and electrophysiological (EEG) variables. We found that behavioural (accuracy = 95.45%), IOS (accuracy = 90.84%) and EEG (accuracy = 88.1%) models showed significantly better performance than the bootstrap condition, establishing the robustness and reliability of these phenotypes in our mouse model (Fig. 5a and b). Importantly, the analysis of feature importance highlighted that the most informative variables are Y maze, IOS amplitude and alpha band (night, active wake) in EEG recordings (Fig. 5c).

Discussion

Quantitative biomarkers measuring cortical function are a fundamental tool for the development of therapeutics, and different techniques have been recently and successfully introduced in clinical and research settings for neurodevelopmental disorders (Bosl *et al.*, 2011;

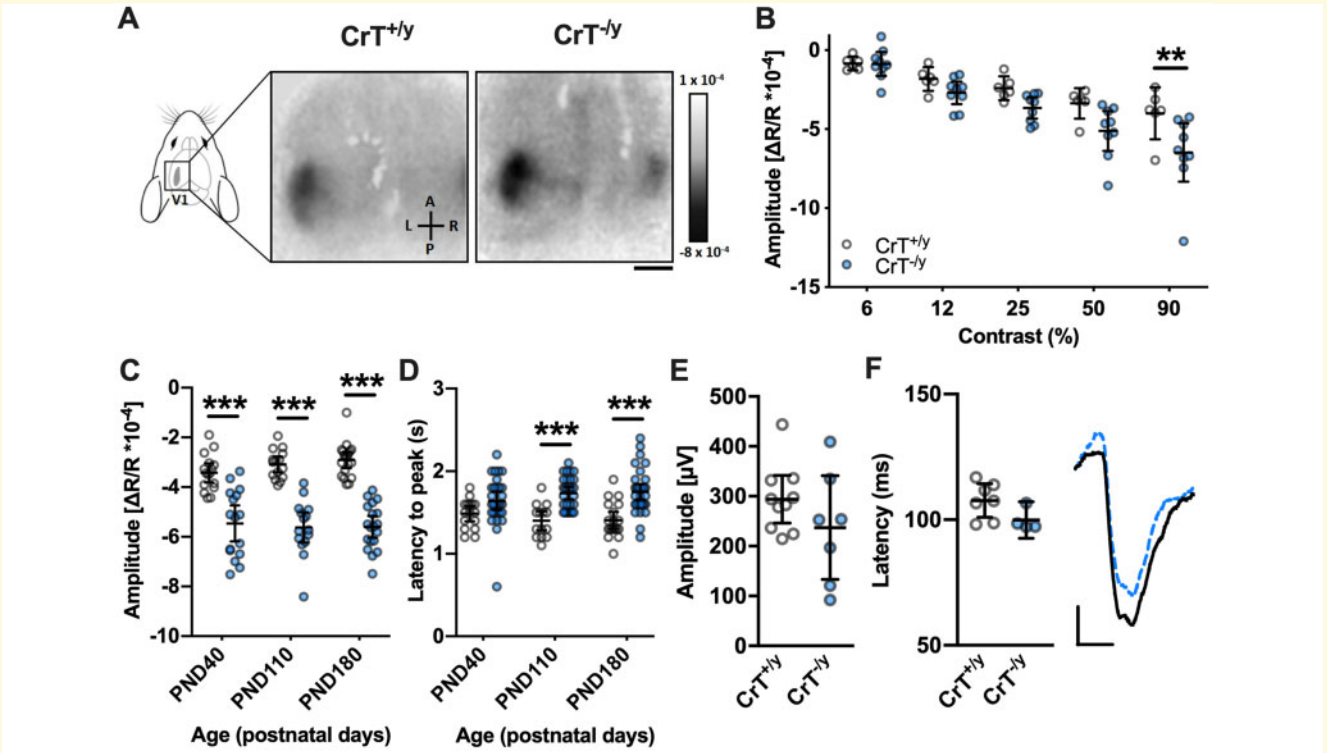

Figure 4 Altered haemodynamic response in CrT$^{-/y}$ animals. (**A**) Typical IOS response to visual stimulation in the binocular visual field for a WT (CrT$^{+/y}$) and a CrT$^{-/y}$ animal. The Look Up Table is shown on the right. Scale bar: 1.8 mm. (**B**) Contrast-response function for contralateral eye stimulation in male WT ($n = 6$) and CrT$^{-/y}$ ($n = 9$) mice at PND40. IOS amplitude was increased in CrT$^{-/y}$ animals in particular at high contrast of visual stimuli (two-way ANOVA, effect of genotype $P < 0.05$, genotype × contrast interaction $P < 0.05$, *post hoc* Holm–Sidak method, $P < 0.01$ at 90% of contrast). (**C**) Response for contralateral eye stimulation in male WT and CrT$^{-/y}$ mice at three different time points (PND40, PND110 and PND180; $n = 15$ for each group at PND40 and PND110, $n = 19$ at PND180). IOS amplitude was significantly increased in CrT$^{-/y}$ animals (two-way ANOVA, effect of genotype $P < 0.001$, *post hoc* Holm–Sidak method, $P < 0.001$ at all ages tested). (**D**) The latency of IOS responses was longer in CrT$^{-/y}$ mice at PND110 and PND180 (two-way ANOVA, effect of genotype $P < 0.001$, *post hoc* Holm–Sidak method, $P < 0.001$). (**E**, **F**) No differences in visually evoked potential amplitude (**E**) and latency (**F**) were detected between WT ($n = 10$) and CrT$^{-/y}$ animals ($n = 7$; *t*-test, $P = 0.767$ and $P = 0.087$, respectively) at PND110. For all panels, circles represent single data values; black lines indicate mean with 95% confidence interval. Representative visually evoked potential traces for a WT (continuous black line) and a CrT$^{-/y}$ (dashed blue line) mouse are also shown on the right. $^{**}P < 0.01$, $^{***}P < 0.001$. Error bars, SEM.

Durand *et al.*, 2012; Jeste *et al.*, 2015; LeBlanc *et al.*, 2015; Boggio *et al.*, 2016; Mazziotti *et al.*, 2017; Sinclair *et al.*, 2017; Bowman and Varcin, 2018; Lupori *et al.*, 2019). Following this approach, we report novel functional biomarkers for creatine transporter deficiency, capable of classifying animal genotypes at single subject level with high accuracy and sensitivity (>85%) and to measure disease progression. These tools may be of high translational value for future preclinical studies of creatine transporter deficiency, and also more broadly for neurodevelopmental disorders presenting with cognitive dysfunction, autistic-like features and brain hyperexcitability.

The clinical relevance of the spectral changes of EEG signal apparent in CrT$^{-/y}$ mice was demonstrated by our findings showing a comparable dysfunction of neural oscillations in creatine transporter deficiency patients. More specifically, theta and alpha power was decreased in the cerebral cortex of CrT$^{-/y}$ mice compared to WT animals, whereas beta and gamma power was increased, highlighting a transition from physiological to pathological network activity similar to that observed in other neurodevelopmental disorders and patients in the autistic spectrum (Jeste *et al.*, 2015; Sinclair *et al.*, 2017). Importantly, theta and alpha bands were altered in the same direction in mice and patients, identifying a possible 'network biomarker' of creatine transporter deficiency disorder. Moreover, we demonstrated that CrT$^{-/y}$ mice display an epileptic phenotype, with spontaneous seizure occurrence and increased susceptibility to kainic acid, as assessed through behavioural observation and video-EEG recordings in awake animals. Since epilepsy is common in creatine transporter deficiency (van de Kamp *et al.*, 2014) and seizures are one of the symptoms with the greatest impact on quality of life of patients and caregivers, these findings fill a gap in the current literature and expand

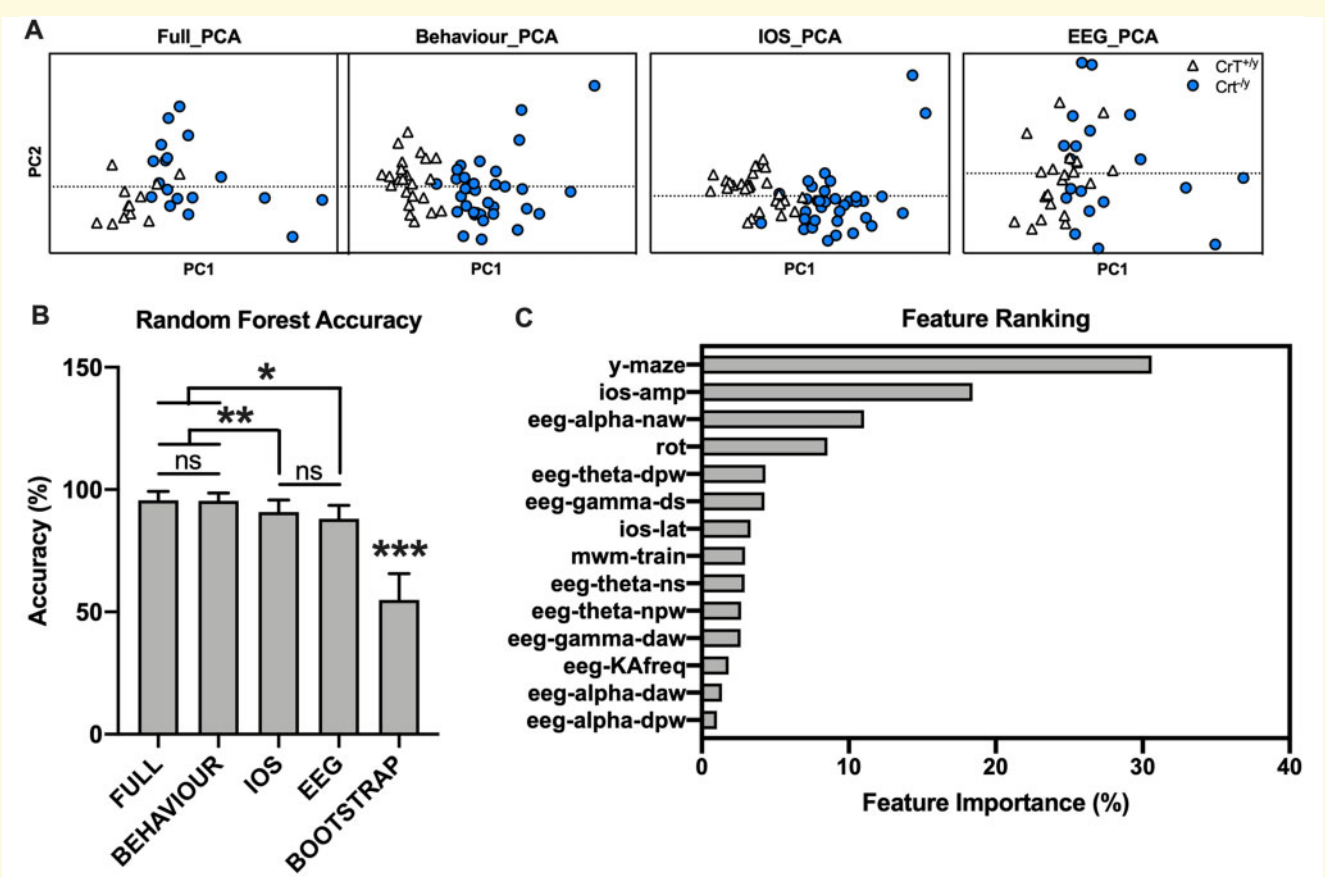

Figure 5 Random Forest analysis of the dataset. (**A**) Scatter plot of all the experimental subjects analysed with the full dataset (Full), behavioural (Behaviour), IOS imaging (IOS) and EEG variables plotted in the space of the first two principal components of principal component analysis. (**B**) Comparison of accuracy for different Random Forest classifiers trained and tested, respectively, with the entire dataset, behavioural, IOS, EEG variables and randomly permuted dataset (Bootstrap). A Kruskal–Wallis analysis followed by Dunn's multiple comparisons revealed that the behavioural variable has an accuracy comparable to the full dataset, whereas the accuracy of IOS and EEG variables is slightly lower. All classifiers displayed a higher accuracy than Bootstrap ($P < 0.001$ for all comparisons). Error bars, standard deviation. (**C**) Histogram depicts the relative importance of top 14 features in the Random Forest model. daw: day active wake; dpw: day passive wake; ds: day sleep; ios-amp: amplitude of IOS; ios-lat: latency of IOS; KAfreq: frequency of seizures after kainic acid challenge; mwm-train: training distance of Morris water maze; naw: night active wake; npw: night passive wake; ns: night sleep; rot: rotarod. *$P < 0.05$, **$P < 0.01$, ***$P < 0.001$, ns, not significant.

the translational validity of our creatine transporter deficiency murine model. The stratification of animals based on the manifestation of spontaneous seizures revealed that epileptic mice exhibit a specific decrease in theta power band with respect to non-epileptic animals. This result is in agreement with previous literature showing that changes in theta band power can be predictive of epilepsy (Bettus *et al.*, 2008; Milikovsky *et al.*, 2017).

Since the timing of rhythmic activity in cortical networks strongly affects the coordination of neuronal responses throughout the cortex, the EEG alterations found in creatine transporter deficiency mice and patients establish a robust link between alterations in brain oscillatory activity and the pervasive cognitive and behavioural impairment of this condition, suggesting that a derangement in local and long-range cortical connectivity and plasticity could be a good candidate to explain at the network level the pathological endophenotype of creatine transporter deficiency (e.g. Jensen and Tesche, 2002; Klimesch *et al.*, 2007; Summerfield and Egner, 2009; Uhlhaas *et al.*, 2009; Jensen and Mazaheri, 2010; Güntekin *et al.*, 2013; Nicolás *et al.*, 2019). The increase in beta and gamma power could seem at odds with the observed cognitive deficits and natural history of creatine transporter deficiency, but excessive beta/gamma activity was previously associated with increased brain excitability and seizures (Willoughby *et al.*, 2003; Maheshwari *et al.*, 2016). In summary, the observed EEG abnormalities may be related to different symptoms in creatine transporter deficiency. Future studies analysing the effects of specific pharmacological approaches (such as anticonvulsant drugs) on EEG components in creatine transporter deficiency patients are needed to further test this notion.

We also found a highly specific increase in cortical IOS responses in $CrT^{-/y}$ mice. Since IOS imaging measures blood oxygenation level-dependent signals, these data

suggest that the assessment of brain metabolic consumption might represent a further non-invasive and sensitive biomarker for the analysis of brain function in creatine transporter deficiency. In light of the ubiquitous expression of *Slc6a8* gene in the brain at the cellular and regional level (Mak *et al.*, 2009), the normal visually evoked potential amplitude recorded in the visual cortex of $CrT^{-/y}$ mice suggests that glial and vascular cells might be the cellular basis of altered IOS. Accordingly, the forced metabolic phenotype and the resultant increase in cellular oxidative stress observed in the brain of $CrT^{-/y}$ animals (Giusti *et al.*, 2019) could dynamically upregulate the cerebral blood flow stimulating vasodilation (Watts *et al.*, 2018). Abnormal neurovascular coupling could significantly affect functional magnetic resonance imaging responses in creatine transporter deficiency patients and represent another creatine transporter deficiency biomarker of relatively easy assessment in children using functional near-infrared spectroscopy (Lloyd-Fox *et al.*, 2010; Vanderwert and Nelson, 2014).

Using a Random Forest machine learning algorithm for data classification, we showed that behavioural, imaging and EEG assessment can be used to automatically classify subjects. Since ease of testing is a key factor in complex multidose assessments, we also showed that smaller subsets of variables could reach a similar discriminative performance.

Overall, our findings identify novel, translational and non-invasive biomarkers for the investigation of brain function in creatine transporter deficiency. Despite the availability of reliable tools for creatine transporter deficiency diagnosis, including biochemical, magnetic resonance spectroscopy and genetic analyses, the biomarkers discovered in this work will have a fundamental impact in the research and clinical setting at multiple levels: (i) their evaluation will allow clinicians to optimize the follow-up of patients, recognizing possible alterations of brain circuits during the progression of creatine transporter deficiency disorder; (ii) the study of EEG pattern could be predictive of the epileptic phenotype; (iii) the combination of behavioural, IOS and EEG testing provides a very reliable protocol to longitudinally monitor the efficacy of potential therapeutic strategies in preclinical, and possibly clinical, studies. It is worth noting that much effort has been invested so far in the research of therapeutic strategies aimed at replenishing brain Cr levels, but efficacy studies of pharmacological approaches targeting specific pathogenetic mechanisms of creatine transporter deficiency disorder need to rely on direct measurements of brain function.

Supplementary material

Supplementary material is available at *Brain Communications* online.

Acknowledgements

We are grateful to Dr Minh-Ha T. Do, Dr John McKew, Dr Eleonora Vannini and Dr Gabriele Sansevero for critical reading of the manuscript and stylistic revision. We thank Francesca Biondi and Elena Novelli for technical support.

Funding

This research was supported by grant GR-2017-02364378 funded by the Italian Ministry of Health, by Telethon grant GGP19177, by grant #1822 funded by Jerome Lejeune Foundation to L.B., and by a grant from Lumos Pharma to T.P. and L.B.

Competing interests

The authors report no competing interests.

References

Baroncelli L, Alessandrì MG, Tola J, Putignano E, Migliore M, Amendola E, et al. A novel mouse model of creatine transporter deficiency. F1000Res 2014; 3: 228.

Baroncelli L, Molinaro A, Cacciante F, Alessandrì MG, Napoli D, Putignano E, et al. A mouse model for creatine transporter deficiency reveals early onset cognitive impairment and neuropathology associated with brain aging. Hum Mol Genet 2016; 25: 4186–200.

Bettus G, Wendling F, Guye M, Valton L, Régis J, Chauvel P, et al. Enhanced EEG functional connectivity in mesial temporal lobe epilepsy. Epilepsy Res 2008; 81: 58–68.

Boggio EM, Pancrazi L, Gennaro M, Lo Rizzo C, Mari F, Meloni I, et al. Visual impairment in FOXG1-mutated individuals and mice. Neuroscience 2016; 324: 496–508.

Bosl W, Tierney A, Tager-Flusberg H, Nelson C. EEG complexity as a biomarker for autism spectrum disorder risk. BMC Med 2011; 9: 18.

Bowman LC, Varcin KJ. The promise of electroencephalography for advancing diagnosis and treatment in neurodevelopmental disorders. Biol Psychiatry Cogn Neurosci Neuroimaging 2018; 3: 7–9.

Cecil KM, Salomons GS, Ball WS Jr, Wong B, Chuck G, Verhoeven NM, et al. Irreversible brain creatine deficiency with elevated serum and urine creatine: a creatine transporter defect? Ann Neurol 2001; 49: 401–4.

Chilosi A, Leuzzi V, Battini R, Tosetti M, Ferretti G, Comparini A, et al. Treatment with L-arginine improves neuropsychological disorders in a child with creatine transporter defect. Neurocase 2008; 14: 151–61.

Dunbar M, Jaggumantri S, Sargent M, Stockler-Ipsiroglu S, van Karnebeek C. Treatment of X-linked creatine transporter (SLC6A8) deficiency: systematic review of the literature and three new cases. Mol Genet Metab 2014; 112: 259–74.

Durand S, Patrizi A, Quast KB, Hachigian L, Pavlyuk R, Saxena A, et al. NMDA receptor regulation prevents regression of visual cortical function in the absence of Mecp2. Neuron 2012; 76: 1078–90.

Dwir D, Giangreco B, Xin L, Tenenbaum L, Cabungcal J-H, Steullet P, et al. MMP9/RAGE pathway overactivation mediates redox dysregulation and neuroinflammation, leading to inhibitory/excitatory imbalance: a reverse translation study in schizophrenia patients. Mol Psychiatry 2019; doi: 10.1038/s41380-019-0393-5.

Fons C, Sempere A, Sanmartì FX, Arias A, Póo P, Pineda M, et al. Epilepsy spectrum in cerebral creatine transporter deficiency. Epilepsia 2009; 50: 2168–70.

Giusti L, Molinaro A, Alessandrì MG, Boldrini C, Ciregia F, Lacerenza S, et al. Brain mitochondrial proteome alteration driven by creatine deficiency suggests novel therapeutic venues for creatine deficiency syndromes. Neuroscience 2019; 409: 276–89.

Güntekin B, Emek-Savaş DD, Kurt P, Yener GG, Başar E. Beta oscillatory responses in healthy subjects and subjects with mild cognitive impairment. Neuroimage Clin 2013; 3: 39–46.

Jaggumantri S, Dunbar M, Edgar V, Mignone C, Newlove T, Elango R, et al. Treatment of creatine transporter (SLC6A8) deficiency with oral S-adenosyl methionine as adjunct to l-arginine, glycine, and creatine supplements. Pediatr Neurol 2015; 53: 360–3.e2.

Jensen O, Mazaheri A. Shaping functional architecture by oscillatory alpha activity: gating by inhibition. Front Hum Neurosci 2010; 4: 186.

Jensen O, Tesche CD. Frontal theta activity in humans increases with memory load in a working memory task. Eur J Neurosci 2002; 15: 1395–9.

Jeste SS, Frohlich J, Loo SK. Electrophysiological biomarkers of diagnosis and outcome in neurodevelopmental disorders. Curr Opin Neurol 2015; 28: 110–6.

Kadam SD, D'Ambrosio R, Duveau V, Roucard C, Garcia-Cairasco N, Ikeda A, et al. Methodological standards and interpretation of video-electroencephalography in adult control rodents. A TASK1-WG1 report of the AES/ILAE translational task force of the ILAE. Epilepsia 2017; 58: 10–27.

Klimesch W, Sauseng P, Hanslmayr S, Gruber W, Freunberger R. Event-related phase reorganization may explain evoked neural dynamics. Neurosci Biobehav Rev 2007; 31: 1003–16.

Kurosawa Y, Degrauw TJ, Lindquist DM, Blanco VM, Pyne-Geithman GJ, Daikoku T, et al. Cyclocreatine treatment improves cognition in mice with creatine transporter deficiency. J Clin Invest 2012; 122: 2837–46.

LeBlanc JJ, DeGregorio G, Centofante E, Vogel-Farley VK, Barnes K, Kaufmann WE, et al. Visual evoked potentials detect cortical processing deficits in Rett syndrome. Ann Neurol 2015; 78: 775–86.

Leuzzi V, Mastrangelo M, Battini R, Cioni G. Inborn errors of creatine metabolism and epilepsy. Epilepsia 2013; 54: 217–27.

Lloyd-Fox S, Blasi A, Elwell CE. Illuminating the developing brain: the past, present and future of functional near infrared spectroscopy. Neurosci Biobehav Rev 2010; 34: 269–84.

Lupori L, Sagona G, Fuchs C, Mazziotti R, Stefanov A, Putignano E, et al. Site-specific abnormalities in the visual system of a mouse model of CDKL5 deficiency disorder. Hum Mol Genet 2019; 28: 2851–61.

Maheshwari A, Marks RL, Yu KM, Noebels JL. Shift in interictal relative gamma power as a novel biomarker for drug response in two mouse models of absence epilepsy. Epilepsia 2016; 57: 79–88.

Mak CSW, Waldvogel HJ, Dodd JR, Gilbert RT, Lowe MTJ, Birch NP, et al. Immunohistochemical localisation of the creatine transporter in the rat brain. Neuroscience 2009; 163: 571–85.

Mancardi MM, Caruso U, Schiaffino MC, Baglietto MG, Rossi A, Battaglia FM, et al. Severe epilepsy in X-linked creatine transporter defect (CRTR-D). Epilepsia 2007; 48: 1211–3.

Mazziotti R, Lupori L, Sagona G, Gennaro M, Della Sala G, Putignano E, et al. Searching for biomarkers of CDKL5 disorder: early-onset visual impairment in CDKL5 mutant mice. Hum Mol Genet 2017; 26: 2290–8.

Mercimek-Mahmutoglu S, Connolly MB, Poskitt KJ, Horvath GA, Lowry N, Salomons GS, et al. Treatment of intractable epilepsy in a female with SLC6A8 deficiency. Mol Genet Metab 2010; 101: 409–12.

Milikovsky DZ, Weissberg I, Kamintsky L, Lippman K, Schefenbauer O, Frigerio F, et al. Theta rhythm alterations—a novel predictive biomarker of epilepsy. J Neurol Sci 2017; 381: 86.

Molinaro A, Alessandrì MG, Putignano E, Leuzzi V, Cioni G, Baroncelli L, et al. A nervous system-specific model of creatine transporter deficiency recapitulates the cognitive endophenotype of the disease: a longitudinal study. Sci Rep 2019; 9: 62.

Müller M, Can K. Aberrant redox homoeostasis and mitochondrial dysfunction in Rett syndrome. Biochem Soc Trans 2014; 42: 959–64.

Nash SR, Giros B, Kingsmore SF, Rochelle JM, Suter ST, Gregor P, et al. Cloning, pharmacological characterization, and genomic localization of the human creatine transporter. Recept Channels 1994; 2: 165–74.

Nelson CA, McCleery JP. Use of event-related potentials in the study of typical and atypical development. J Am Acad Child Adolesc Psychiatry 2008; 47: 1252–61.

Nicolás B, Sala-Padró J, Cucurell D, Santurino M, Falip M, Fuentemilla L. Theta rhythm supports hippocampus-dependent integrative encoding in schematic memory networks. 2019; doi: 10.1101/2019.12.16.874024.

Póo-Argüelles P, Arias A, Vilaseca MA, Ribes A, Artuch R, Sans-Fito A, et al. X-linked creatine transporter deficiency in two patients with severe mental retardation and autism. J Inherit Metab Dis 2006; 29: 220–3.

Racine RJ. Modification of seizure activity by electrical stimulation. II. Motor seizure. Electroencephalogr Clin Neurophysiol 1972; 32: 281–94.

Rose S, Niyazov DM, Rossignol DA, Goldenthal M, Kahler SG, Frye RE. Clinical and Molecular characteristics of mitochondrial dysfunction in autism spectrum disorder. Mol Diagn Ther 2018; 22: 571–93.

Schiaffino MC, Bellini C, Costabello L, Caruso U, Jakobs C, Salomons GS, et al. X-linked creatine transporter deficiency: clinical description of a patient with a novel SLC6A8 gene mutation. Neurogenetics 2005; 6: 165–8.

Sinclair D, Oranje B, Razak KA, Siegel SJ, Schmid S. Sensory processing in autism spectrum disorders and Fragile X syndrome-From the clinic to animal models. Neurosci Biobehav Rev 2017; 76: 235–53.

Skelton MR, Schaefer TL, Graham DL, Degrauw TJ, Clark JF, Williams MT, et al. Creatine transporter (CrT; Slc6a8) knockout mice as a model of human CrT deficiency. PLoS One 2011; 6: e16187.

Summerfield C, Egner T. Expectation (and attention) in visual cognition. Trends Cogn Sci 2009; 13: 403–9.

Udobi KC, Kokenge AN, Hautman ER, Ullio G, Coene J, Williams MT, et al. Cognitive deficits and increases in creatine precursors in a brain-specific knockout of the creatine transporter gene Slc6a8. Genes Brain Behav 2018; 17: e12461.

Uhlhaas PJ, Pipa G, Lima B, Melloni L, Neuenschwander S, Nikolić D, et al. Neural synchrony in cortical networks: history, concept and current status. Front Integr Neurosci 2009; 3: 17.

Valayannopoulos V, Boddaert N, Chabli A, Barbier V, Desguerre I, Philippe A, et al. Treatment by oral creatine, L-arginine and L-glycine in six severely affected patients with creatine transporter defect. J Inherit Metab Dis 2012; 35: 151–7.

van de Kamp JM, Mancini GM, Salomons GS. X-linked creatine transporter deficiency: clinical aspects and pathophysiology. J Inherit Metab Dis 2014; 37: 715–33.

Vanderwert RE, Nelson CA. The use of near-infrared spectroscopy in the study of typical and atypical development. NeuroImage 2014; 85: 264–71.

Watts ME, Pocock R, Claudianos C. Brain energy and oxygen metabolism: emerging role in normal function and disease. Front Mol Neurosci 2018; 11: 216.

Willoughby JO, Fitzgibbon SP, Pope KJ, Mackenzie L, Medvedev AV, Clark CR, et al. Persistent abnormality detected in the non-ictal electroencephalogram in primary generalised epilepsy. J Neurol Neurosurg Psychiatry 2003; 74: 51–5.